Concentric-Tube Continuum Robot for Infrastructure Inspection

Cindy Zhong, Joseph Koh, Mark Long, Tyler Wilson

September 2023 to April 2024

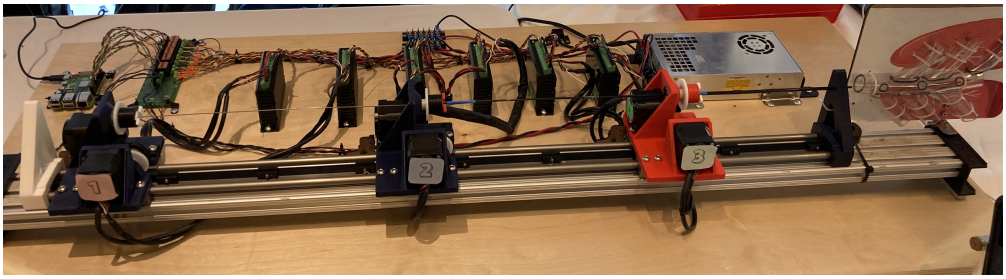

Executive Summary

Concentric Tube Continuum Robots (CTCR) are soft and compliant robots composed of concentric elastic tubes, pre-curved to allow for dexterous movement. Their ability to conform to their environment unlike traditional rigid robots and the compact size of their tubes makes CTCRs advantageous for confined environments. CTCRs offer promise in a wide range of applications, such as endoscopy and minimally invasive surgery, and search and rescue and exploration in cluttered spaces by mounting a camera or end-effector on its tip. However, due to their compliant nature, it is challenging to precisely control the tip of CTCR robots. Under our sponsor Prof. Kefei Wen of the Department of Mechanical Engineering at the University of British Columbia, our team seeks to build a CTCR and develop and implement precise and novel controls (both classical physics-based and machine learning), for the purpose of infrastructure pipe inspections.

During the first year of our project, we designed and built the hardware of our CTCR such that it satisfies the requirements from our sponsor. Namely, our CTCR is a "six-degree of freedom" robot, meaning one can fully control the position and the orientation of our CTCR's tip, which is crucial to inspect pipes with a camera. We have designed our CTCR's hardware such that it will be possible to control the position with precision comparable to the current gold standard, which is necessary to develop sophisticated controls of the tip. Finally, our robot was built well within the budget (less than $1500), which is considerably cheaper than a leading open-source model Grassmann et al. (2024).

A key insight from our CTCR thus far is that while the hardware (e.g. motors, mechanical build) may be built to precision, other areas - specifically the tubes and techniques for calibration - will need to be further developed to benefit from the high precision of the hardware.

Our recommendations for this project's next steps, which we plan to implement in the next year of our project, are to upgrade our tubes to the industry-standard material, Nickel Titanium (Nitinol), implement a more precise calibration and tip tracking system, and apply physics-based and machine learning control methods. Key challenges ahead include accurately pre-curving the Nitinol tubes to the desired shape, and designing calibration and tip tracking systems, which we will need to research further.

Contents

1 Introduction **5**

2 Project Overview **6**

2.1 Project Requirements 6

2.2 Proposed Solution . . . 7

3 Discussion **8**
3.1 Mechanical Design . . . 8
3.2 Electrical Configuration . . . 12
3.3 Selection of Tubes . . . 14
3.3.1 Tube Material . . . 14
3.3.2 Shape-Setting of Tubes . . . 15
3.3.3 Tube Pairs . . . 17
3.4 Robotic Control . . . 19

4 Conclusions **21**

5 Recommendations **22**

6 Deliverables **23**

A Motor Calculations **24**
A.1 Motor Resolution Specification . . . 24
A.2 Total Torque Equation . . . 25
A.3 Tube Rotation Motor - Required Torque . . . 25
A.4 Tube Translation Motor - Required v.s. Delivered Force at Rack and Pinion Interface 26

B Dominating Stiffness Modelling **26**

C Tube Optimization Computations **28**
C.1 Tube Deflection Calculations . . . 28
C.2 Tube Diameter Optimization Code . . . 30
C.3 Tube Length and Curvature Optimization Code . . . 31

D Bill of Materials **32**

References **33**

List of Figures

1 Continuum robots with extrinsic actuation . . . 5
2 System overview of concentric tube robot . . . 7
3 Different classifications of CTCR actuation units . . . 8
4 CRL open-source parallel-architecture CTCR . . . 9

5 Translation motor force requirement 10
6 Motor precision requirement 10
7 Exploded view of a single actuation block 11
8 CAD of our 6 DOF CTCR 12
9 Electrical setup for the robot 13
10 Tube in joule heating setup 16
11 Spring back of Nitinol tubes for furnace heating compared to electrical heating . . . 16
12 Comparison of dominating-stiffness and balanced-stiffness tube pairs 18
13 Tip differences between theoretical zero-clearance model and nonzero-clearance models for different clearance values and coefficients of friction 19
14 Visualization of the tube parameter optimization process 19
15 High-level control algorithm for the robot 21
16 Dominating stiffness implementation for forward and inverse kinematic 22
17 CRL open-source parallel-architecture CTCR 25
18 Extension lengths are inputs to the dominating stiffness model 27
19 Sketch of deflection forces on the tubes 29
20 Inverse kinematic process 31
21 Tube parameter optimization process 31

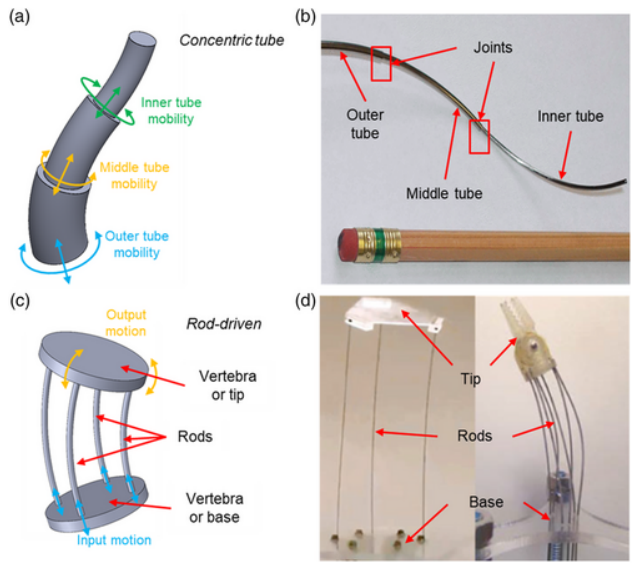

Figure 1: Continuum robots with extrinsic actuation: concentric tube robots, a) with their mobility and b) a prototype; rod-driven continuum robots, c) with a conceptual scheme and d) a parallel continuum robot prototype

Russo et al. (2023)

1 Introduction

When many people think of robotics the first thing that may come to mind is something that might resemble the Boston Dynamics robotic dog or a six-degrees-of-freedom robotic arm. These and most other commonly seen robots are examples of *rigid robots* which are characterized by a finite number of joints with rigid connections between them. The counterpart to rigid robots is known as *soft robots*. One particular category of soft robotics is *continuum robots* which are robots with infinitely many joints where motion is generated from deflection.

Concentric-tube continuum robot (CTCR) is a kind of continuum robot, as shown in Fig. 1. It is made of pre-curved tubes nested inside each other and whose shape is controlled by translating and rotating each tube independently (Russo et al. (2023)). Since the tubes are made of compliant materials (often Nitinol, a Ni-Ti alloy), the robot can conform to complex shapes as their curvatures interact non-linearly.

There are on-going research on applying CTCR in minimal invasive surgery (MIS) due to its compliant to the immediate surrounding and dexterity of motion to navigate the human anatomy. This was first suggested by Sears and Dupont (2006) in their design of a steerable needle technology. A review paper by Burgner-Kahrs et al. (2015) provides a comprehensive list of research done in this area and their milestones. More recent advances can be found in Dupont et al. (2022).

This project, however, concerns with the application of continuum robot outside of the medical field

—in particular, for infrastructure inspection. We elaborate the project goals in more details in the subsequent sections.

2 Project Overview

2.1 Project Requirements

Our sponsor, Prof. Kefei Wen, is interested in developing a concentric tube continuum robot that can be used to perform research on control methods of continuum robotics as well as to collaborate with the UBC Civil Engineering Department for pipe inspection.

Through early discussion with our sponsor, we agreed on the project scope outlined in Table 1. This scope details what we wish to accomplish at the end of the second year of work on this project and satisfies our sponsor's requirements to perform future research with this project.

Item	**Must-haves**	**Soft-requirements**
Mechanical system	Durable (components do not need replacing within two years of use) Ease of maintenance for operator	Compact linear design
Control	Less than 2% tip position error	Reliable performance
Range of motion	6 degrees-of-freedom	
Tubes	Can support camera Tubes retain their shape after being stressed	Diameter as small as possible Inner tubes are compliant to outer tubes
Workspace	Can extend around 20 cm Can navigate within a small S-shaped pipe	Can be generalized to operate well in different work environments
Cost	Less than $1,500	

Table 1: Scope Table

Our model will make use of three tubes. Each tube has the capacity of being rotated and linearly extended, providing two degrees of freedom for each tube. To maximize the working space of our robot we will opt for a three-tube design, providing a possible six degrees of freedom.

A reliable performance can be achieved by minimizing the tip position error, defined in Eq. (1). Knowing the exact location of the tip position is a nontrivial inverse kinematics problem. Current methods for control of concentric tube robots report tip position errors of approximately between 1% and 3% with current research being done on how to reduce this further. Error can also arise from the mechanical system either from mechanical inconsistencies, such as backlash, or from the resolution of the motors. Specific care must be taken to avoid mechanical inconsistencies while the resolution should be specified so that the resolution error does not dominate the control error.

To ensure this is the case, a goal of less than 2% tip position error was specified in Table 1.

$$e_{\text{tip}} = \frac{\|x_d - x_a\|}{L}, \quad \begin{cases} e_{\text{tip}} = \text{tip position error} \\ x_d = \text{desired tip position} \\ x_a = \text{actual tip position} \\ L = \text{maximum extension length of robot} \end{cases} \tag{1}$$

2.2 Proposed Solution

To meet our specifications, our robot design features three actuation units to control the translation and rotation of the tubes with each unit in charge of two degrees of freedom per tube. A camera will be mounted on the tip of the robot for visual feedback and data and users can interface with the system via command line for teleoperation. A system-level diagram of our robot can be referred to in Fig. 2.

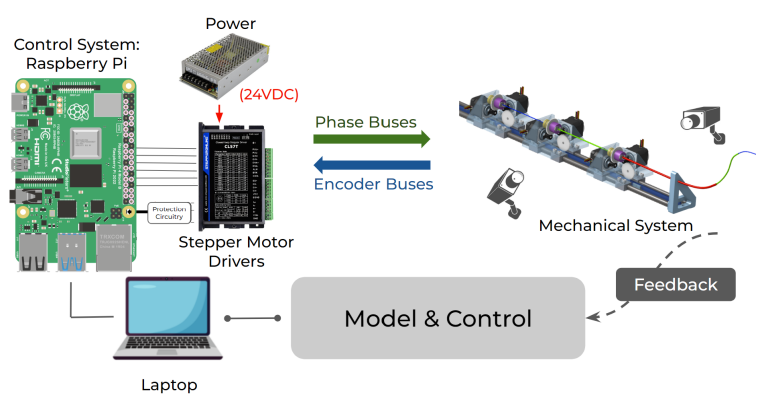

Figure 2: System overview of concentric tube robot

1. **Mechanical System**: Three actuation units each driven by two stepper motors each to offer six degrees of freedom in total and to fulfill the resolution requirements.
2. **Electrical System**: A power distribution set-up to distribute 24V DC power source to the robot and a control board to send the Raspberry Pi signals to the stepper motor drivers.
3. **Control System**: The entire system is controlled by a Raspberry Pi which sends out signals to actuate the tubes. We can manipulate the speed, the distance traveled, and the amount of rotation the robot does. Three limit switches are used home the translation of our robot.
4. **Tubes**: Three concentric tubes consisting of flexible material to bend and twist into different shapes to navigate complex systems.

We will discuss in detail how each system component helps to achieve our project goal in the following sections.

3 Discussion

3.1 Mechanical Design

Since the primary objective of this project is to develop a CTCR with six degrees of freedom (DOFs) control of the tip, the first design consideration is the number of tubes, which determines the number of DOFs. Each pre-curved tube provides two DOFs by translating through extension and retraction and rotating about its longitudinal axis under the influence of attached actuators. Therefore we proceed with three pre-curved concentrically-fitted tubes to attain six DOFs control of the tip.

There are three types of CTCR architectures: parallel, serial, hybrid, and serial (Fig. 3) which determine which DOFs are coupled or independent. Unlike in serial or hybrid, all the DOFs in parallel architectures are independent, eliminating the possibility of error propagation between DOFs. We thus select parallel architecture to reduce error, to help achieve our requirement of precise tip control.

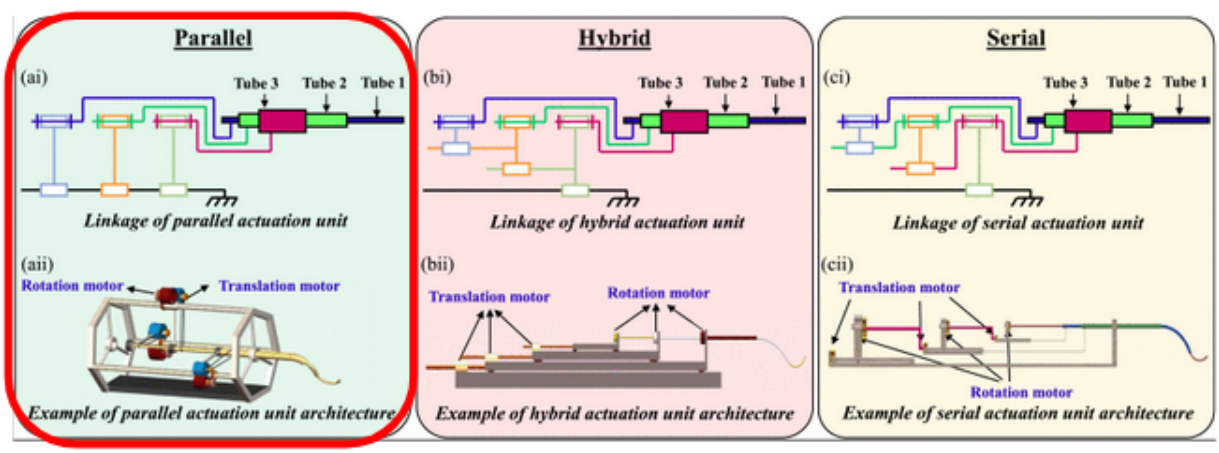

Figure 3: Different classifications of CTCR actuation units. All six actuation units (DOFs) are independent in a parallel architecture (a), only the three translation units are coupled in a hybrid architecture (b), and all six units are coupled in a serial architecture (c).

Nwafor et al. (2023)

The Continuum Robotics Laboratory (CRL) at the University of Toronto has developed open-source parallel-architecture CTCR hardware (Fig. 4). To reduce risk so to complete the robot build within the time constraints of our project, we adopt their CTCR design.

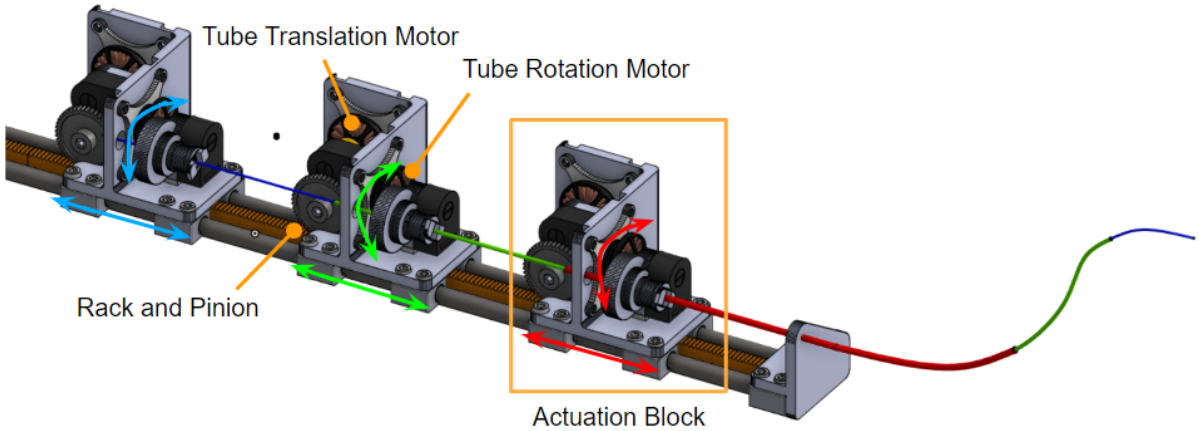

Figure 4: CRL open-source parallel-architecture CTCR. BLDC motors serve as the actuation units; for each tube, one BLDC motor rotates the tube via a gear train, while another translates the tube and the actuation block via a rack and pinion.

Grassmann et al. (2024)

However, the CRL's design employs BLDC motors (as the CTCR's actuation units), drivers, and encoders with a cost (>$2500 CAD) beyond our budget. Therefore, we seek more affordable alternatives to these components. To meet our high-level objectives (Table 1), our new motors and drivers must satisfy the following criteria:

1. **Affordable (total cost of motors, drivers, and encoders <$500 CAD)** to keep the overall CTCR cost within the $1500 budget.

2. **Sufficient torque (safety factor $\geq$ 5, required torque value depends on motor mass)** for desired motion of the tubes and actuation blocks. The translation motor must supply enough torque (varies based on motor weight) to overcome friction as it moves the actuation block across the rails (Fig. 5) while the rotational motor must supply enough torque to rotate the tubes in their fully extended state. We choose a high safety factor to account for sources of friction that are difficult to accurately predict (e.g. friction between the tubes). See Appendix A for calculations.

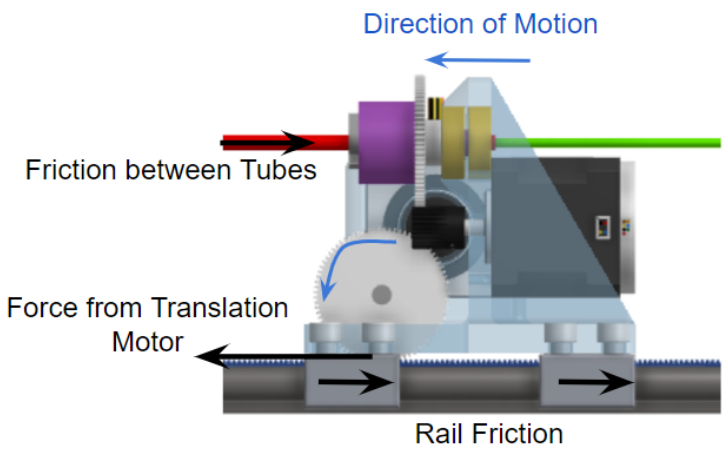

Figure 5: Translation motor force requirement. The motor must provide sufficient torque to overcome friction between the rails and tubes, and translate the actuation block.

3. **Sufficient resolution (Output of >3200 steps/revolution after gear ratio)** to make our high-level minimum tip increment requirement (<2% of full tube extension length) attainable (Fig. 6). The required motor resolution of >3200 steps/revolution permits a theoretical tip resolution of error <0.2%, ensuring that that the lower bound on the error comes from the control method instead of the mechanical setup (See Appendix A for calculations).

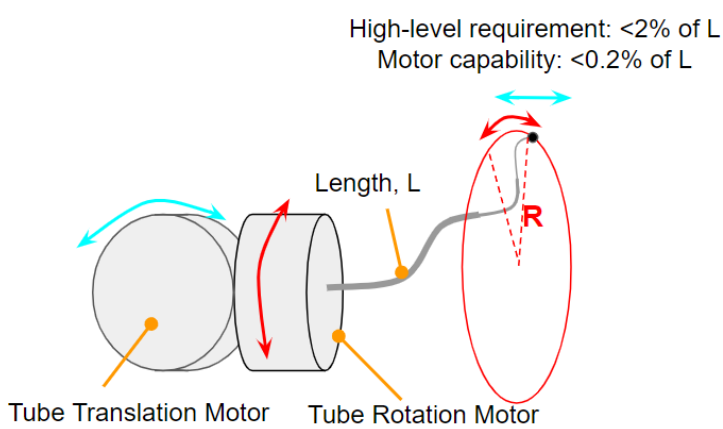

Figure 6: Motor precision requirement. Each motor must have a resolution high enough to provide a minimum increment in tip position.

4. **Compact (Nema 23 or smaller, smaller is better)** to keep our CTCR compact in size.

We find that this Nema 17 Closed Loop Stepper Motors satisfies the above criteria when we mount

a 40:12 gear train from the stepper's shaft to the tube or rack (Fig. 7), and run the stepper at eight microsteps per full step.

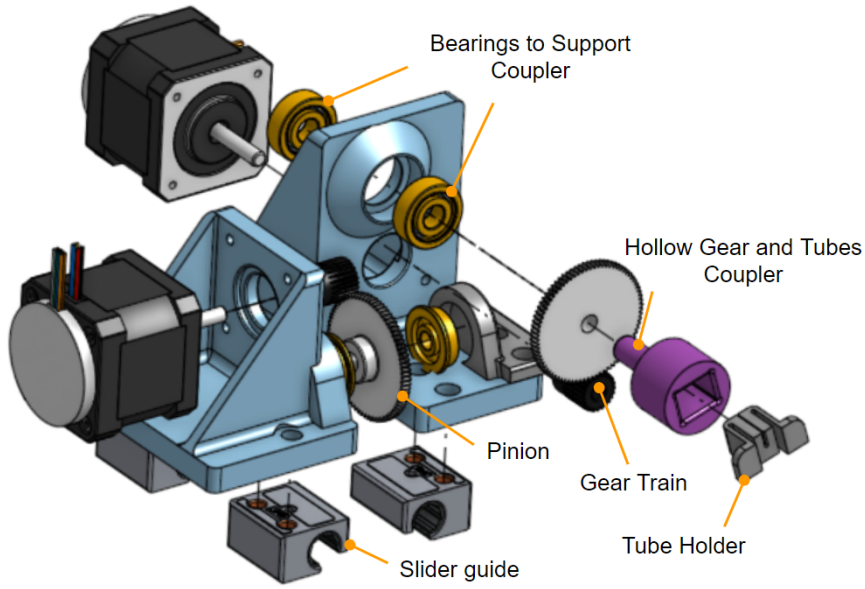

Figure 7: Exploded view of a single actuation block. A sub-assembly of bearings, gears, and couplers transfers torque from one motor to rotate the tubes, while a similar sub-assembly transfers torque from another motor to translate the tubes.

We then modify several other components of the CRL's assembly to incorporate the new motors and to ensure precise control. For example, we add second bearings to both the tube rotation coupler and to the translation pinion to reduce shaft precession (Fig. 7). Additionally, during fabrication we ensure the press fit between the coupler and gear and the tube holder and tube are especially tight since our encoder, which only records the stepper motor's shaft movement (being integrated into our steppers), will not observe slipping at these interfaces, which would thus result in a loss of tip accuracy.

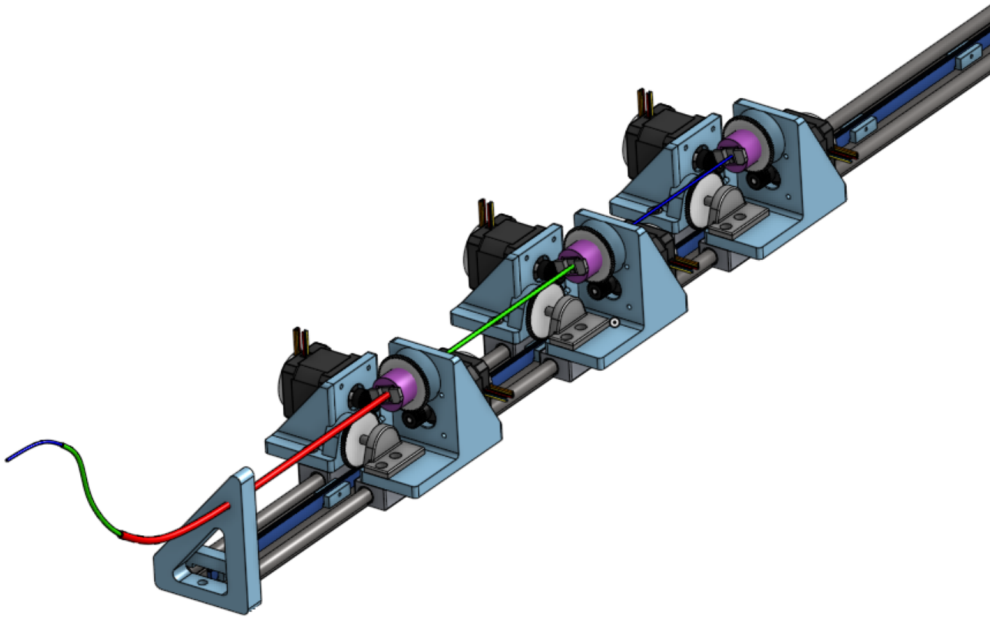

Figure 8: CAD of our 6 DOF CTCR. For each tube, one BLDC motor rotates the tube via a gear train, while another translates the tube and the actuation block via a rack and pinion.

3.2 Electrical Configuration

The electrical subsystem is designed to ensure the required stepping resolution and ease of operation and maintenance in the future. We chose CL57T stepper motor drivers to simplify our system, although designing our own driver board could minimize space usage. Nevertheless, we avoided a custom PCB to meet project deadlines and simplify future debugging and maintenance, as off-the-shelf drivers provide comprehensive manuals and hardware debugging features.

The CL57T driver also reads the encoder bus to close the position control loop so we do not have to process the encoder signals ourselves, reducing the need for additional circuitry and control code.

The electrical circuit to control one stepper motor is shown in Fig. 9b. According to the stepper motor user manual (StepperOnline (2023)), a lower operating voltage (24VDC) is desired at a lower speed to reduce motor heating and vibration. A stepper driver draws current near the motor's rated maximum to maintain consistent torque for precise stepping. Therefore, we selected a power supply to provide well above 9A at 24VDC (each motor draws 1.5A).

We chose the Raspberry Pi Model 4B as our controller for its ability to run Python code, increased RAM, and robust multimedia and networking capabilities, essential for integrating camera feeds, teleoperation, and multiple sensors in the project's next stage.

(a) CL57T Closed-loop stepper driver

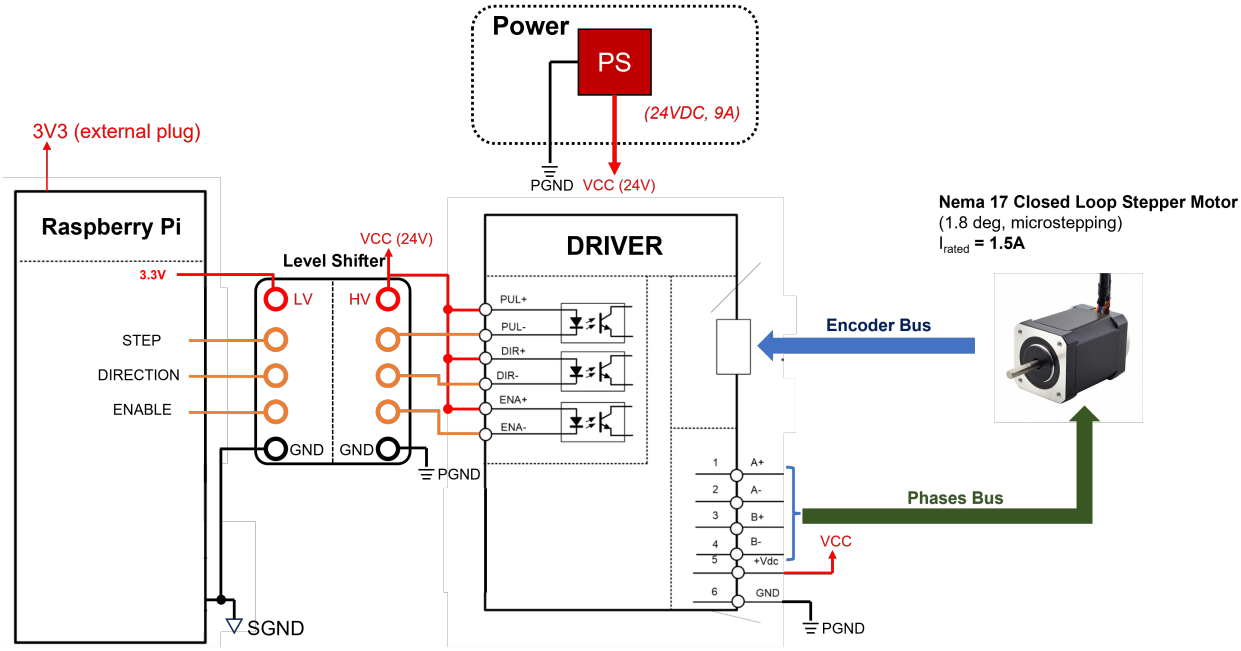

(b) Electrical schematic to drive one stepper motor

Figure 9: Electrical setup for the robot. Note the full network includes six motors and six drivers.

The Pi is powered via an external adapter and outputs 3V3 logic. We made a practical decision to use level shifters to convert the control signal to 24V. This choice aligns with the driver's acceptance of this level and the voltage being provided to the motors. As a result, we can route the power supply directly to the high side of the level shifters, eliminating the need for any buck converters.

We adjust the actuation speed by modifying the pulse frequency, with a maximum outlined in the timing diagram in the motor driver manual (StepperOnline (2023)). Since our focus is on position control rather than speed, a moderate actuation speed is sufficient. After several trials, we set the base frequency at approximately 400 Hz, which minimizes vibration and maintains a reasonable translation speed of 4 mm/s.

On the prototype robot, grounds from the motors are tied in a star configuration to limit ground loops. The system includes other minor components that were not discussed here, such as limit switches.

Together, by opting for an off-the-shelf closed-loop stepper driver and streamlining the circuitry —such as using 24V logic to eliminate the need for a buck converter— we designed an electrical setup that is cost-efficient, requires few extra components, supports the future addition of camera and sensors, and is easy to operate and maintain.

3.3 Selection of Tubes

3.3.1 Tube Material

Many different possible tube combinations are possible as each tube can have different lengths, curvature functions, diameters, textures, and materials. Significant research has been conducted on how changing these tube properties can affect the performance of these robots Nwafor et al. (2023). Specifying the lengths, curvatures, and diameters is important for characterizing the range of motion and workspace of the robot. Referring to Table 1, the tubes that we select must be durable and reliable but we do not have any strict requirements on the workspace our robot must be able to navigate. Based on these requirements, the material we choose for our tubes will be the most important consideration. Because workspace characterization is not as big of a consideration and we will likely be purchasing all of our tubes from the same supplier for ease of production, we defined the following simplifying assumptions for our design process:

1. All tubes will be made of the same material
2. All tubes will be untextured
3. All tubes will be of piecewise-constant curvature

A literature review of many different types of continuum tube robots evaluated the different types of materials that can be used for the tubes. Nitinol tubes are currently the gold standard. 3D printed, heat-shrink, and polymer-based tubes were also explored, however, while being more affordable, these options typically have significantly shorter lifespans than nitinol, and in the case of the 3D printed tubes, the resolution of the tubes during manufacturing was a possible concern. A common property of all the options listed above is they are all superelastic, meaning that they can undergo large strains (6-8% in the case of nitinol) without any plastic deformation. This is a necessity as the tubes are likely to undergo large strains during use. Nitinol tubes proved to be more durable than other superelastic materials and are also biocompatible, meaning that they can safely enter the body and be used in medical applications Dupont et al. (2010). We explored the use of other flexible metals that would have a comparable lifespan but were not able to find any that were superelastic or that were mentioned in any literature. For these reasons, our team determined that Nitinol tubes would be most optimal to satisfy our criteria.

3.3.2 Shape-Setting of Tubes

We will require curved tubes for the robot to fully explore the workspace. There are two primary ways to curve Nitinol tubes:

1. Furnace heating
2. Joule heating

Both processes involve setting the tube to the desired shape and heating it to temperatures ranging between around $400°$C and $550°$C and holding it at that temperature for some fixed amount of time (usually between 2 and 20 minutes) Baron (2022); Gilbert and Webster (2016); Matthey (2024). Furnace heating involves placing the tube into a ceramic mold and inserting it into a furnace to complete the process while joule heating also involves creating a mold (commonly laser cut or 3D printed) and running a high-ampere current through the tube to heat it. No one method has been definitively proven to be better than the other and both have their advantages and faults Dupont et al. (2010).

We explored the option of having the tubes be pre-bent for us by the suppliers to avoid overhead but the associated cost was outside our budget. The method by which we will bend the tubes is an active area of research. The joule heating method outlined by Gilbert and Webster (2016) is the most promising approach that we have found at this time Fig. 10. It involves using current and voltage sensing to monitor the resistance which is used as a proxy for the temperature. This process was compared to a furnace heating method such as one outlined in Yip et al. (2023) and utilized more readily available equipment, faster experiment times, and less spring back from the desired shape Fig. 11.

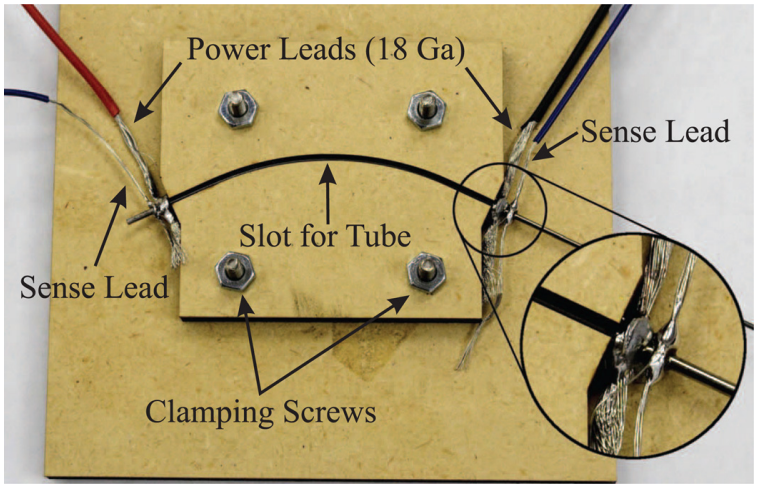

Figure 10: Tube in joule heating setup
Gilbert and Webster (2016)

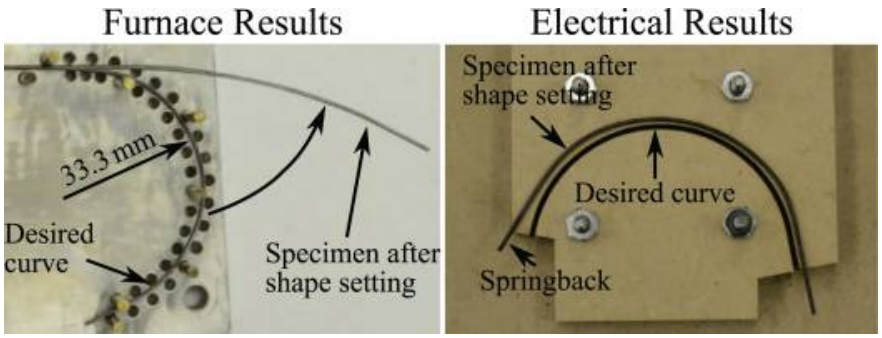

Figure 11: Spring back of Nitinol tubes for furnace heating compared to electrical heating
Gilbert and Webster (2016)

Current risks associated with shape-setting the tubes are that if the material is heated too much then it risks losing its microstructure or losing its superelastic properties Baron (2022) which is why we chose the material in the first place. The material properties are slightly different depending on the alloy of Nitinol used which can affect the optimal temperature that should be used. Insufficient heating will result in more spring back in the shape-setting process. This can be mitigated by repeating the experiment Gilbert and Webster (2016). Overheating the tubes can be mitigated by temperature monitoring and tuning the experiment for the specific alloy of Nitinol we purchase.

3.3.3 Tube Pairs

The tube design of three-tube concentric tube robots involves the tubes being nested inside one another with the innermost tube being called the "distal" tube and the outermost tube being called the "proximal" tube. During forward motion, the proximal tube extends first and the distal tube extends last to reach the desired endpoint. Depending on the relative stiffnesses of the tubes, we will see slightly different behavior during this extension. Two main tube pairs may be used:

1. Dominating-stiffness tube pair
2. Balanced-stiffness tube pair

A visual of these models is displayed in Fig. 12. Naturally, most tube pairs will not be perfectly one or the other, however, depending on how we select the stiffness ratio between the two tubes, denoted by D, we can come up with tube pairs that more closely resemble one or the other. A perfect dominating-stiffness pair implies that the tubes are kinematically decoupled. The balanced-stiffness pairing also typically leads to higher torsional and frictional forces which leads to discrepancies in the theoretical model and the actual positions of the tubes Dupont et al. (2010). For these reasons, we will choose to select dominating-stiffness pairings for our tubes. A recommended dominating stiffness ratio between adjacent tubes is 10 with values of 6-8 being proven sufficient on the lower and values of 20 being used on the higher end Bergeles et al. (2015).

We opted to follow this recommendation and select a stiffness ratio of $D = 10$. This value falls close to many other past examples. We decided not to choose a value too much larger than the nominal as it would lead to less compliance in the tubes and higher stress values which could introduce a higher risk of the tubes breaking. A value too low would allow the tubes to be too compliant, compromising control accuracy. Additionally, because the proximal tubes are first to extend during motion, and are more stiff, a higher stiffness ratio would lead to increased stability of the robot through its extension phase.

How to choose an appropriate clearance distance between tubes is not a heavily researched area and there do not appear to be many physical experiments comparing and contrasting different clearance values. However, there is some research on how the clearance values affect the tip

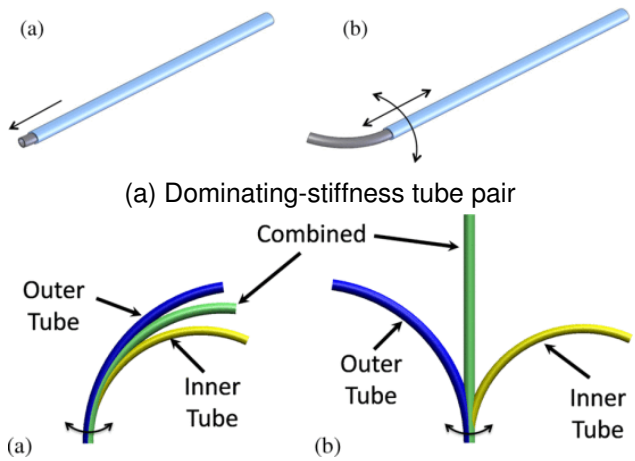

(a) Dominating-stiffness tube pair

(b) Balanced-stiffness tube pair

Figure 12: Comparison of dominating-stiffness and balanced-stiffness tube pairs
Dupont et al. (2010)

position error in sophisticated theoretical models detailed in Fig. 13. The figure implies that low clearances increase tip position error with increasing values of coefficients of friction. The coefficient of friction between nitinol tubes is 0.6 under dry conditions and can be 0.1 or lower with lubrication feng ZENG et al. (2012); Zeng and Dong (2013).

If we select the middle value of $\mu = 0.3$ for our purpose a clearance of 0.2mm or 0.3mm appears to be optimal. We will select the slightly larger value of 0.3mm to reduce the risk of higher bending and frictional forces damaging our tubes and to reduce mechanical uncertainty within our tubes. Given ideal clearance values and dominating stiffness ratios, we can relate the diameters between tube pairs. This means that once we choose the diameters for one tube, we can compute the ideal diameters for all other tubes. Given that we plan to mount a camera on the end of the distal tube, we must also ensure that the tube is sufficiently stable enough to support the weight of the camera. This means that the tube must deflect no more than some amount when fully extended. This allowed us to set a lower bound on how thin our tubes could be for a given robot length as well as provide an additional constraint that can be used in selecting the optimal diameters for our tubes. Detailed computations and simulation code are supplied in Appendix C.1 and Appendix C.2.

Along with selecting the diameters of the tubes, we will also need to determine the optimal extension lengths, curved lengths, and curvature values of the tubes for a given workspace. The workspace we're considering is an S-shaped pipe with arbitrary dimensions where we are aiming to be able to have our robot get close to the edge of the pipe and point normal to the surface so that the camera on the end of the tube can get a good view of the sides of the pipe anywhere along the surface. To choose the tube parameters that would best accomplish this, we created a set of test points consisting of a tip location and orientation we want the robot to achieve. An inverse

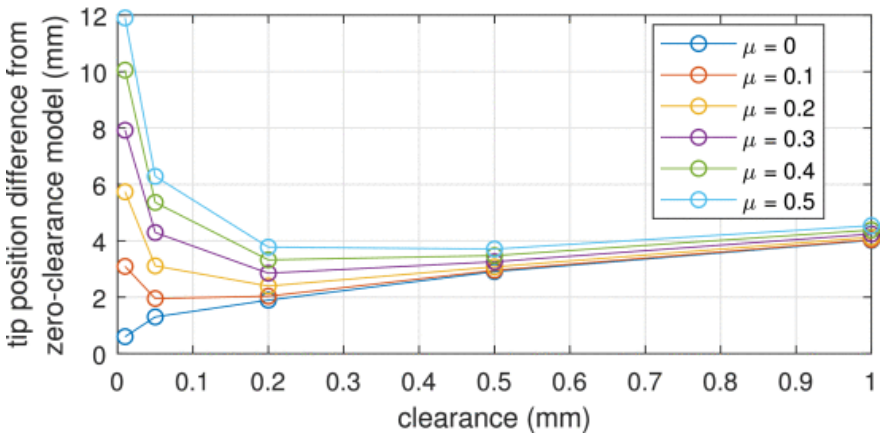

Figure 13: Tip differences between theoretical zero-clearance model and nonzero-clearance models for different clearance values and coefficients of friction
Liu et al. (2023)

kinematic method using the dominating stiffness physics-based model was used to navigate the robot as close to the desired test point as possible. The mean squared error between the actual and desired position and orientation for each of these test points was measured and minimized to select the optimal tube parameters. This process is visualized in Fig. 14 while code and more detail on the approach used can be found in Appendix C.3.

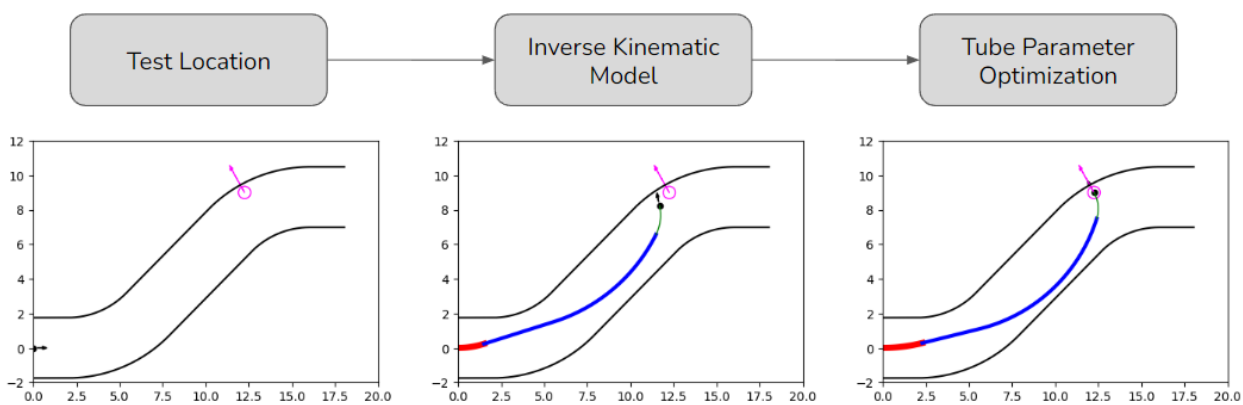

Figure 14: Visualization of the tube parameter optimization process

3.4 Robotic Control

Control research done this year and context of what are we doing next year Controlling the robot involves two key aspects: modeling and control algorithm. First, we need a model that translates the six motors' positions into the tubes' 3D location, orientation, and shape. The control algorithm uses this model and incorporates feedback to complete the control loop.

Modeling a CTCR is complex due to the need to account for elastic tube interactions. Although torsion and bending are governed by linear second-order differential equations, such as the Euler-Bernoulli beam theory (Wikipedia (2023)), the interactions between tubes' curvatures make the model of a concentric-tubes system highly non-linear (Sears and Dupont (2006)).

		Physics-based			**Data-based**
		Dominating Stiffness	Constant Curvature	Cosserat Rod Theorem	Machine Learning
Include?	Bending	No	Yes	Yes	N/A
	Torsion	No	Yes	Yes	N/A
Error (% of total length)		$>$3%	3%	1%	$<$1%
Reference		Sears and Dupont (2006)	Sears and Dupont (2006), Webster III and Jones (2010)	Alqumsan et al. (2019)	Grassmann et al. (2022a)

Table 2: Modelling approaches in current literature

Table 2 outlines existing modeling approaches. From left to right, the complexity and accuracy of a model increases as it takes into account mutual bending and torsion between the tubes. However, these models are often too computationally expensive to simulate and be used in real-time control (Alqumsan et al. (2019)).

A model of the robot provides the approximate forward and inverse kinematics required for a control algorithm, as illustrated in Fig. 15.

We acquired this illustration through consultation with Dr. Steven Lilge from the University of Toronto. Directly using inverse kinematics to configure motor positions for desired tube locations and orientations is impractical. Instead, employing the Jacobian form of inverse kinematics allows the robot to incrementally approach its target pose. This stepwise adjustment is more feasible than attempting to achieve precise motor configurations in one go.

Feedback mechanisms vary; teleoperation uses real-time camera feeds for human-guided adjustments, while autonomous control processes these feeds with computer vision algorithms. Although these methods provide real-time positioning, they don't account for the robot's shape, making accurate path planning reliant on a robust robot model. However, in applications like pipe inspection, occasional contact with the pipe interior is acceptable as long as the robot's tip reaches the intended location.

We have implemented the dominating stiffness model (Fig. 16) as detailed in Appendix B, though

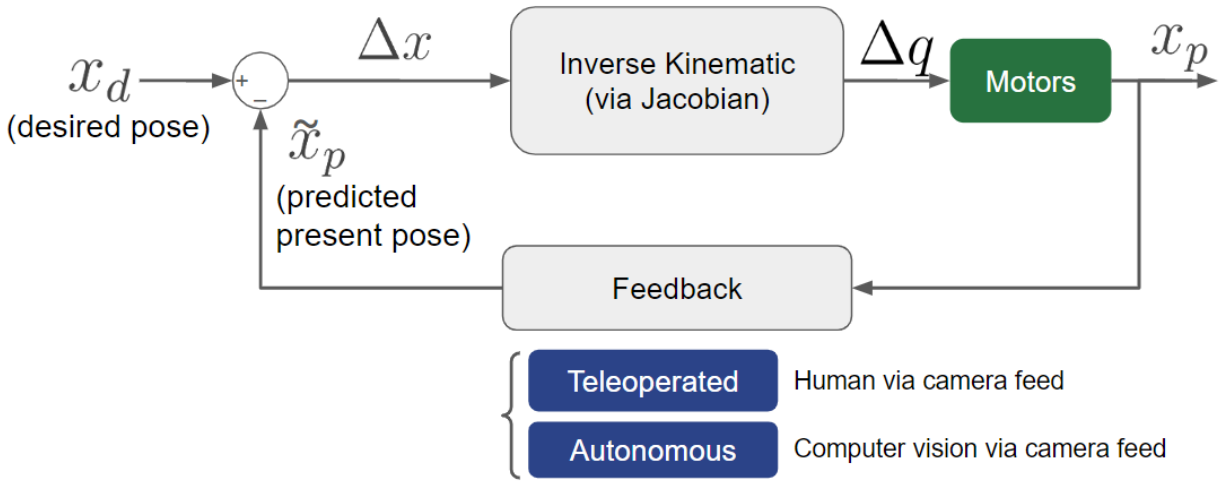

Figure 15: High-level control algorithm for the robot. More details to be studied in the coming year.

its utility is untested due to our prototype's non-compliance with the stiffness assumption. Next year, we plan to adopt the constant curvature model to better account for mutual bending effects in tubes of similar stiffness. It is not currently clear whether Cosserat Rod Theorem provides significant added accuracy since mutual torsion affects the pose much less.

In summary, we have familiarized ourselves with the concepts and challenges of continuum robot modelling. A simple dominating stiffness model and open loop control were implemented. In the coming year, we will focus on more advanced modelling and incorporating feedback into the system. The main goal is to achieve intuitive teleoperated control for infrastructure inspection. Time permitting, we will also explore autonomous control and machine learning for the modelling problem.

4 Conclusions

Closing out the first year of this project, our team was able to fully design and assemble a novel design for a concentric tube robot with many competitive advantages over the leading open-source models. Our robot was designed to support tip precision of error tolerance as low as 0.2%. This is smaller than the error from the leading control methods, meaning that the lower bound on the error would come from the control method instead of the mechanical setup which means that our robot can operate with the same precision as the current best models. Furthermore, our robot costs less than $1500 in total which is considerably cheaper than the open-source design without losing any resolution or precision.

To properly validate all of the criteria outlined in Table 1 we will need to use higher-quality tubes

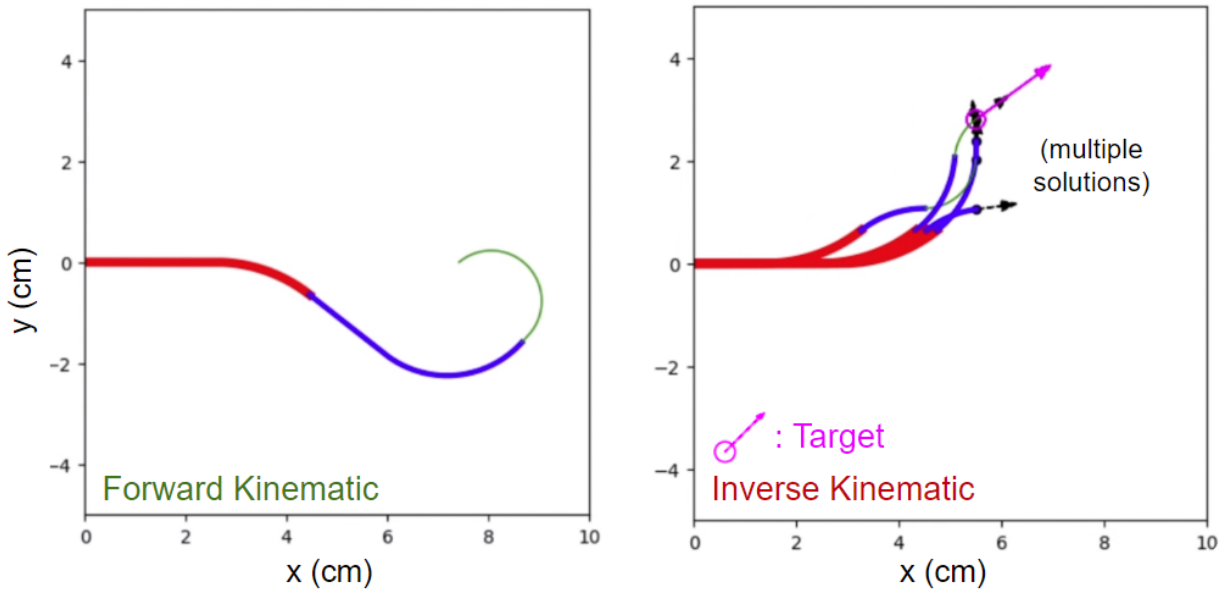

Figure 16: Dominating stiffness implementation for forward and inverse kinematic

to produce experiments with more reliability. This would allow us to determine the mechanical reliability of our robot along with making benchmarks of the error. Furthermore, this will allow us to construct a physics-based model of our robot to implement various control methods next year such as open-loop control and closed-loop control where we will integrate two orthogonal cameras to capture the final tip position of our robot. However, a significant risk remains regarding curving the Nitinol tubes.

5 Recommendations

There are three main recommendations from our work on the design, construction, and control of the prototype this year.

- **Pay more attention to the science of tube's material:** We recommend that future work (including the continuation of our project) gives much greater attention to the material properties of the tubes and the physics that governs their behaviour. After the difficulty of obtaining Nitinol tubes, we opted for plastic tubes and piano wires for our first-year demonstration. However, it was quickly acknowledged that these materials often behave unreliably or unpredictably due to weak material integrity, buckling, and springback. These effects made reliable control infeasible. Even when Nitinol tubes are used, there should be comprehensive testing of the materials under normal and extreme operating conditions -only then can we confidently move on to the modeling and control of the robot itself.

- **Identify mechanical hardware errors that can overshadow the high resolution of the stepper motors' motions:** After building the prototype, we realized that there is more uncertainty in the mechanical design than we have accounted for (placement of limit switch, click distance of limit switch's handle, placement of tube holder, the length of tubes, etc). Given that we aim for high accuracy and specify our system components according to that goal, we should have a better understanding of the various sources of hardware uncertainty and their magnitude. Otherwise, it would be difficult to determine if an observed error is from the control algorithm or from a biased hardware setup.
- **Design of rotation homing requires more research:** Currently, we have not implemented a robust homing mechanism for tube rotations. This problem is quite non-trivial since the consistent homing of the motor shaft along is not enough -one must also consider the placement of the tube itself onto the motor shaft and whether its orientation can be consistently reproduced. We are planning an electrical homing system (rather than mechanical via limit switch) for higher accuracy, but more research is needed.

By addressing the above recommendation, our sponsor (or, our team) could confidently go forward with the modeling and control of the robot for infrastructure inspection.

6 Deliverables

1. Onshape CAD
2. Github Repo
3. Colab Motor Calculations
4. Link to tube optimization simulation

A Motor Calculations

In this section, we discuss the calculations we did to determine the required specifications for our motors. From these calculations we conclude that this Nema 17 17HS15-1504-ME1K closed loop stepper motor in combination with a 40:12 gear ratio satisfies our requirements (Section 3.1).

Please refer to this Python notebook for the complete calculations. Below is an explanation and sketch of the calculations, and the results from the code. Please note, that all the quantities below have metric units.

A.1 Motor Resolution Specification

Standard stepper motors can increment the angle at 0.9 or 1.8 degrees per step (Motion (2023b)). The steppers from StepperOnline, our supplier of interest, increment at 1.8 degrees per step. This means a resolution of (360degrees/1.8degrees) steps per revolution = 200 steps per revolution. Considering that our rotational maximum radius (i.e. robot length, 20cm) will be much larger than our pinion radius (2cm), and assuming we use a similar gear ratio as the Continuum Robotics Laboratory for both our rotational and translational stages (before pinion), we can conclude that if rotation resolution is sufficient, translational resolution must be too.

Given that in the literature, the robot tip can travel with accuracy of 1.5-3% of robot length Grassmann et al. (2022b), we want to design the motors such that if the tubes were rigid, the smallest possible change in tangential distance travelled by the tip would ideally be at least 0.2% of robot length, $(2E{-}3){\times}L$ (Fig. 6). Tangential resolution of the tip is $(\text{minimum achievable angular increment}){\times}L$. Thus, we want $(\text{minimum achievable angular increment}){\times}L < 2E{-}3{\times}L$ or simplified, minimum achievable angular increment $<$ 2E-3 radians.

Results

- Achieving a resolution $<$.2% is equivalent to a resolution $\geq$3142 steps per revolution.
- Stepper motors that 1.8 degrees per full step have a resolution of 200 steps per revolution.
- Assuming the stepper runs 8 microsteps per full step, achieving 3142 steps per revolution requires gear ratio of at least 2.

The microstepping by a factor of 8 was chosen taking into account resolution, torque, and accuracy needs.

A.2 Total Torque Equation

Peak Torque (T_P) Requirement

The peak, or maximum torque required for the application, can be calculated by summing the load torque (T_L), torque due to inertia (T_J) and the torque required to overcome the friction (T_F).

There are other factors which will contribute to the overall peak torque requirements. For example, the windage loss which is contributed by the resistance offered by the air in the air gap. These factors are complicated to account for. Therefore, a 20% safety margin is given as a rule of thumb when calculating the torque.

EQUATION 2:

$$\therefore T_P = (T_L + T_J + T_F) * 1.2$$

The torque due to inertia (T_J) is the torque required to accelerate the load from standstill or from a lower speed to a higher speed. This can be calculated by taking the product of load inertia, including the rotor inertia and load acceleration.

EQUATION 3:

$$T_J = J_{L+M} * \alpha$$

where:

J_{L+M} is the sum of the load and rotor inertia and α is the required acceleration

The mechanical system coupled to the motor shaft determines the load torque and the frictional torque.

Figure 17: Equations to determine the torque required from a motor given the load, inertia, friction, and angular acceleration.

Yedamale (2003)

A.3 Tube Rotation Motor - Required Torque

How much torque does our motor for rotating the tubes have to handle?

Considering turning up tube fully extended, turned 90 degrees from axis, in horizontal plane (maximal torque situation). Instead of finding the mass of three separate hollow tubes, we consider the outermost tube filled in with nitinol for a simplified overestimation of tube mass:

Results

- The maximum load torque due to camera and tube weight for tube rotation is 0.0413 Nm

- The acceleration torque is 0.0131 Nm
- Instead of calculating the frictional torque (between tubes) and the load torque due to inner tube torsion, we simplify our calculations using a high factor of safety on the load torque due to weight and acceleration torque. Therefore, we approximate that the torque our motors for rotating the tubes should be able to deliver after gear ratio is 0.272 Nm

A.4 Tube Translation Motor - Required v.s. Delivered Force at Rack and Pinion Interface

This one is a bit more complicated than tube rotation, because the force required varies, depending on the weight of the motors Fig. 5. Because we are microstepping the motors, our holding torque is reduced using the formula:

$$\text{incremental holding torque} = \text{full stepping torque} \times \frac{\sin(90^\circ)}{\text{number of microsteps per step}} \tag{2}$$

(Motion (2023a))

Results Gathering the above, and calculating the required and theoretical torques and resolutions of multiple motors, we conclude that the smallest motor that supplies sufficient torque and resolution is this Nema 17 17HS15-1504-ME1K closed loop stepper motor in combination with a 40:12 gear ratio. It has the following specifications:

- required resolution (minimum tip deviation to robot length): 0.2%
- resolution after 8x microstep, gear ratio (minimum tip deviation to robot length): 0.118%
- required force at rack and pinion: 1.987 N
- maximum force applicable at rack and pinion: 14.63 N
- actual max acceleration: 14.45 $\mathrm{m/s^2}$
- max output torque: 0.2926 Nm
- required output torque for tube rotation (after SF=5): 0.2722 Nm

B Dominating Stiffness Modelling

The code for the dominating stiffness model can be found in the following GitHub repo.

Methodology:

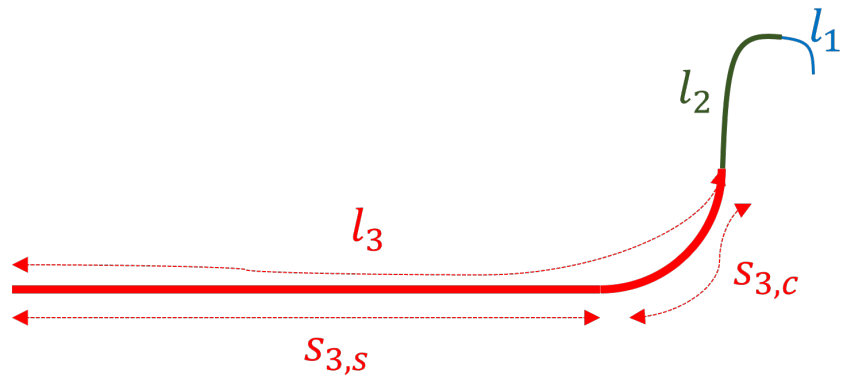

Figure 18: Extension lengths are inputs to the dominating stiffness model

We assume that for any pair of tubes, the shape and curvature of the outer tube will dictate that of the inner tube. Effectively, the outermost tube dictates the shape of the inner two and the middle tube dictates the shape of the innermost tube. When an inner tube extrudes outside of the outer tube, however, it retains its natural curvature.

Then, to find the shape of the concentric tube system, we only need to know how much each tube is extended.

Forward Kinematic via Dominating Stiffness

Input:

- Tube parameters ($i = 1, 2, 3$, 3 is the outermost tube): $\kappa_i = 1/r_i$ (where r_i is the radius of curvature) , $l_{c,i}$ (length of tube that is curved) , L_i (total length of tube)
- Kinematic inputs: θ_i (rotation angle), l_i (extension length)

Output: Shape of robot, location, and orientation of the tip.

For each tube i with extension length l_i, let s_{i_s} be the extended length of the straight segment and $s_{i,c}$ be the length of the extended curved segment, as illustrated in Fig. 18, then we have:

$$s_{i,s} = \max(0, l_i - l_{ic})$$
$$s_{i,c} = l_i - s_{i,s}$$

We will work in 2D for now and generalization to 3D should be straight forward (just adding rotation in/out of the page).

First, we define the follow two functions in 2D. They map a point from origin to its new coordinate after following a straight or curved path of length s.

$$\begin{bmatrix}0\\0\end{bmatrix} \rightarrow f(s) = \begin{bmatrix}s\\0\end{bmatrix} \qquad \begin{bmatrix}0\\0\end{bmatrix} \rightarrow g(\kappa, s) = \frac{1}{\kappa}\begin{bmatrix}\sin(\kappa s)\\1-\cos(\kappa s)\end{bmatrix}$$

Also, let $R(\theta)$ denotes the rotation matrix in 2D:

$$R(\theta) = \begin{bmatrix}\cos\theta & -\sin\theta\\ \sin\theta & \cos\theta\end{bmatrix}$$

Then, the location of the tip is given by:

$$\vec{u} = f(s_{3,s}) + g(\kappa_3, s_{3,c}) + R(\kappa_3 s_{3,c})(f(s_{2,s}) + g(\kappa_2, s_{2,c}) + R(\kappa_2 s_{2,c})(f(s_{1,s}) + g(\kappa_1, s_{1,c})))$$

And the tangential (orientation) vector of the tip is given by:

$$\hat{n} = \prod_{i=1}^{3} R(\kappa_i s_{i,c}) \begin{bmatrix}1\\0\end{bmatrix}$$

Inverse Kinematic via Dominating Stiffness In the inverse problem, given tip position $\vec{u}$ and orientation $\hat{n}$, find l_i and θ_i for $i = 1, 2, 3$.

Since we are in 2D, each $theta_i$ can only be $0\,\mathrm{deg}$ or $180\,\mathrm{deg}$. Due to reflection symmetry, we can fix $\theta_1 = 0\,\mathrm{deg}$. Then we need 5 equations in total. However, we only have 4 independent equations from $\vec{u}$ and $\hat{n}$ via the forward kinematic equations. Thus, we fix $\theta_2 = 0\,\mathrm{deg}, 180\,\mathrm{deg}$ each time to get a different solution.

The system of equations is solved numerically using Nelder–Mead method, and the solutions for a particular target is shown in Fig. 16.

C Tube Optimization Computations

C.1 Tube Deflection Calculations

We wish to ensure that the maximum deflection of our tubes is less than some fixed amount. If our tubes deflect too much they cannot self-support, meaning that we have a restricted workspace and more exaggerated effects in the tip position error due to any mechanical vibrations. We computed a theoretical worst-case tip deflection for our tubes, assuming that all the tubes are fully extended

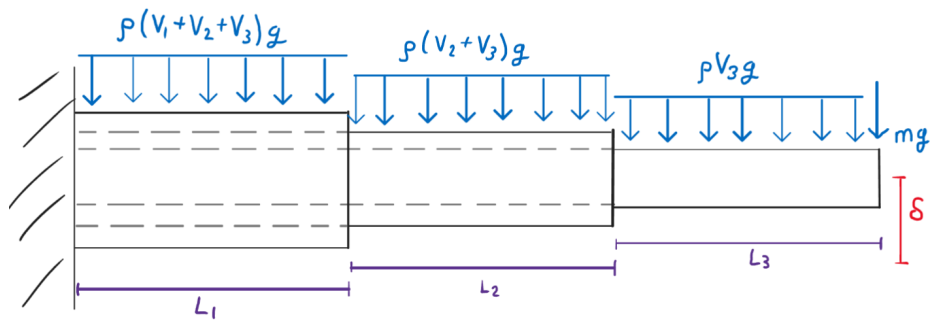

Figure 19: Sketch of deflection forces on the tubes

and perfectly straight, cantilever beams. Taking curvature into consideration would result in the beams' center of mass being closer to the point of support and we would expect less deflection. Thus, this assumption would provide a theoretical upper bound for the static deflection.

To compute the deflection δ we utilized Castigliano's Theorem with three concentric tubes of stiffnesses I_1, I_2, I_3, and mass density ρ with a mass m on the end of the distal tube as shown in Fig. 19.

$$P = mg$$

$$\delta = \frac{\partial U}{\partial P}$$

$$U = \int_0^{L_1+L_2+L_3} \frac{M^2}{2EI} dx$$

$$\delta = \frac{1}{E} \int_0^{L_1+L_2+L_3} \frac{M}{I} \frac{\partial M}{\partial P} dx$$

$$\rho = \frac{m}{V} \Rightarrow m = \rho V = \rho A x$$

$$M(x) = -Px - \frac{1}{2}\rho A_1 g x^2 - \frac{1}{2}\rho A_2 g (x - L_1)^2 \mathbb{1}\{x > L_1\} - \frac{1}{2}\rho A_3 g (x - L_1 - L_2)^2 \mathbb{1}\{x > L_1 + L_2\}$$

$$\frac{\partial M}{\partial P} = -x$$

$$I(x) = I_1 + I_2 \mathbb{1}\{x > L_1\} + I_3 \mathbb{1}\{x > L_1 + L_2\}$$

$$\delta = \frac{1}{E} \left(\int_0^{L_1} \frac{M}{I} \frac{\partial M}{\partial P} dx + \int_{L_1}^{L_1+L_2} \frac{M}{I} \frac{\partial M}{\partial P} dx + \int_{L_1+L_2}^{L_1+L_2+L_3} \frac{M}{I} \frac{\partial M}{\partial P} dx \right)$$

$$\int_0^{L_1} \frac{M}{I} \frac{\partial M}{\partial P} dx = \int_0^{L_1} \frac{mgx^2 + \frac{1}{2}\rho A_1 g x^3}{I_1} dx = \frac{g}{I_1} \left(\frac{mL_1^3}{3} + \frac{\rho A_1 L_1^4}{8} \right)$$

$$\int_{L_1}^{L_1+L_2} \frac{M}{I} \frac{\partial M}{\partial P} dx = \int_{L_1}^{L_1+L_2} \frac{mgx^2 + \frac{1}{2}\rho A_1 g x^3 + \frac{1}{2}\rho A_2 g x (x - L_1)^2}{I_1 + I_2} dx$$

$$= \frac{g}{I_1 + I_2} \left(\frac{m((L_1 + L_2)^3 - L_1^3)}{3} + \frac{\rho A_1 ((L_1 + L_2)^4 - L_1^4)}{8} \right)$$

$$+ \frac{g\rho A_2}{I_1 + I_2} \left(\frac{(L_1 + L_2)^4 - L_1^4}{8} - \frac{(L_1 + L_2)^3 - L_1^3}{3} L_1 + \frac{(L_1 + L_2)^2 - L_1^2}{4} L_1^2 \right)$$

$$\int_{L_1+L_2}^{L_1+L_2+L_3} \frac{M}{I} \frac{\partial M}{\partial P} dx = \int_{L_1+L_2}^{L_1+L_2+L_3} \frac{mgx^2 + \frac{1}{2}\rho A_1 g x^3 + \frac{1}{2}\rho A_2 g x (x - L_1)^2 + \frac{1}{2}\rho A_3 g x (x - L_1 - L_2)}{I_1 + I_2 + I_3} dx$$

$$= \frac{g}{I_1 + I_2 + I_3} \left(\frac{m((L_1 + L_2 + L_3)^3 - (L_1 + L_2)^3)}{3} + \frac{\rho A_1 ((L_1 + L_2 + L_3)^4 - (L_1 + L_2)^4)}{8} \right)$$

$$+ \frac{g\rho A_2}{I_1 + I_2 + I_3} \left(\frac{(L_1 + L_2 + L_3)^4 - (L_1 + L_2)^4}{8} - \frac{(L_1 + L_2 + L_3)^3 - (L_1 + L_2)^3}{3} L_1^2 + \frac{(L_1 + L_2 + L_3)^2 - (L_1 + L_2)^2}{4} L_1^2 \right)$$

$$+ \frac{g\rho A_3}{I_1 + I_2 + I_3} \left(\frac{(L_1 + L_2 + L_3)^4 - (L_1 + L_2)^4}{8} - \frac{(L_1 + L_2 + L_3)^3 - (L_1 + L_2)^3}{3} (L_1 + L_2) + \frac{(L_1 + L_2 + L_3)^2 - (L_1 + L_2)^2}{4} (L_1 + L_2)^2 \right)$$

Following the steps in the work above, the theoretical worst-case deflection is given by Eq. (3). This value is dependent on the specific extension lengths and stiffnesses of each tube. The stiffness of a tube can be related to the inner and outer diameters of the tube using Eq. (4)

$$\begin{aligned}\delta = \frac{g}{E}\Bigg(&\frac{1}{I_1}\left(\frac{mL_1^3}{3}+\frac{\rho A_1 L_1^4}{8}\right)+\frac{1}{I_1+I_2}\left(\frac{m((L_1+L_2)^3-L_1^3)}{3}+\frac{\rho A_1((L_1+L_2)^4-L_1^4)}{8}\right)\\
&+\frac{\rho A_2}{I_1+I_2}\left(\frac{(L_1+L_2)^4-L_1^4}{8}-\frac{(L_1+L_2)^3-L_1^3}{3}L_1+\frac{(L_1+L_2)^2-L_1^2}{4}L_1^2\right)\\
&+\frac{1}{I_1+I_2+I_3}\left(\frac{m((L_1+L_2+L_3)^3-(L_1+L_2)^3)}{3}+\frac{\rho A_1((L_1+L_2+L_3)^4-(L_1+L_2)^4)}{8}\right)\\
&+\frac{\rho A_2}{I_1+I_2+I_3}\left(\frac{(L_1+L_2+L_3)^4-(L_1+L_2)^4}{8}-\frac{(L_1+L_2+L_3)^3-(L_1+L_2)^3}{3}L_1+\frac{(L_1+L_2+L_3)^2-(L_1+L_2)^2}{4}L_1^2\right)\\
&+\frac{\rho A_3}{I_1+I_2+I_3}\left(\frac{(L_1+L_2+L_3)^4-(L_1+L_2)^4}{8}-\frac{(L_1+L_2+L_3)^3-(L_1+L_2)^3}{3}(L_1+L_2)+\frac{(L_1+L_2+L_3)^2-(L_1+L_2)^2}{4}(L_1+L_2)^2\right)\Bigg)\end{aligned} \tag{3}$$

$$I = \frac{\pi}{64}(d_o^4 - d_i^4) \tag{4}$$

C.2 Tube Diameter Optimization Code

To determine the optimal diameters for our tubes we need to systematically solve for six unknowns: $d_{1,i}, d_{1,o}, d_{2,i}, d_{2,o}, d_{3,i}, d_{3,o}$. This means that we will require six unknowns to determine the optimal values. We determined the clearance values between tubes to be $C = 0.3$ mm in Section 3.3.3 which relates the diameters by Eq. (5), giving us two equations.

$$d_{k,i} = d_{k+1,o} + 2C \tag{5}$$

The dominating stiffness ratio of $D = 10$ we chose gives us the relationship in Eq. (6). Combining this with Eq. (4) we get Eq. (7) which gives another two equations that relate the diameters.

$$D = \frac{I_k}{I_{k+1}} \tag{6}$$

$$d_{k,0} = \sqrt[4]{D(d_{k+1,o}^4 - d_{k+1,i}^4) + d_{k,i}^4} \tag{7}$$

We can get one more equation by stipulating that the deflection defined in Eq. (3) must be smaller than some value. This gives us our fifth constraint. While this is not enough to fully define all of our parameters, it greatly reduces our parameter space, making it easy to select tube pairs. Using the Young's modulus and mass density for Nitinol given by (Euroflex (2021)) and fixing one of our arbitrary dimensions to be that the outer diameter of the distal tube should be half of the diameter of the endoscopic camera that we chose we were able to produce optimal diameters through the following code.

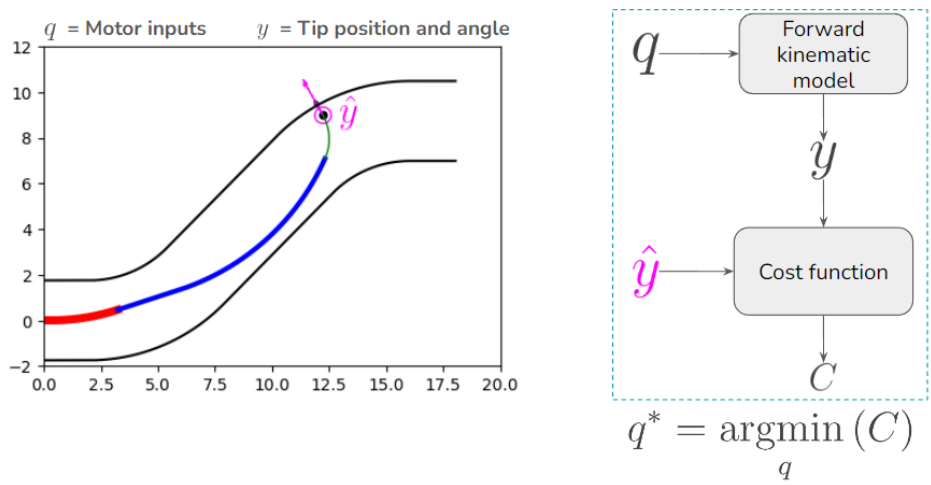

Figure 20: Inverse kinematic process. The test point with angle and orientation is shown in purple and denoted by $\hat{y}$. The optimal motor inputs are denoted by q^* and are found by minimizing the error expressed in the cost function.

C.3 Tube Length and Curvature Optimization Code

The inverse kinematic model is one component in how we determine the optimal tube parameters for a workspace. When given a test point (position and orientation) we want to determine what the motor (or kinematic) inputs should be to our system to get as close as possible to this point. This is defined to be the inverse kinematic method and is described at a high level by the process outlined in Fig. 20 with a detailed analysis found in Appendix B.

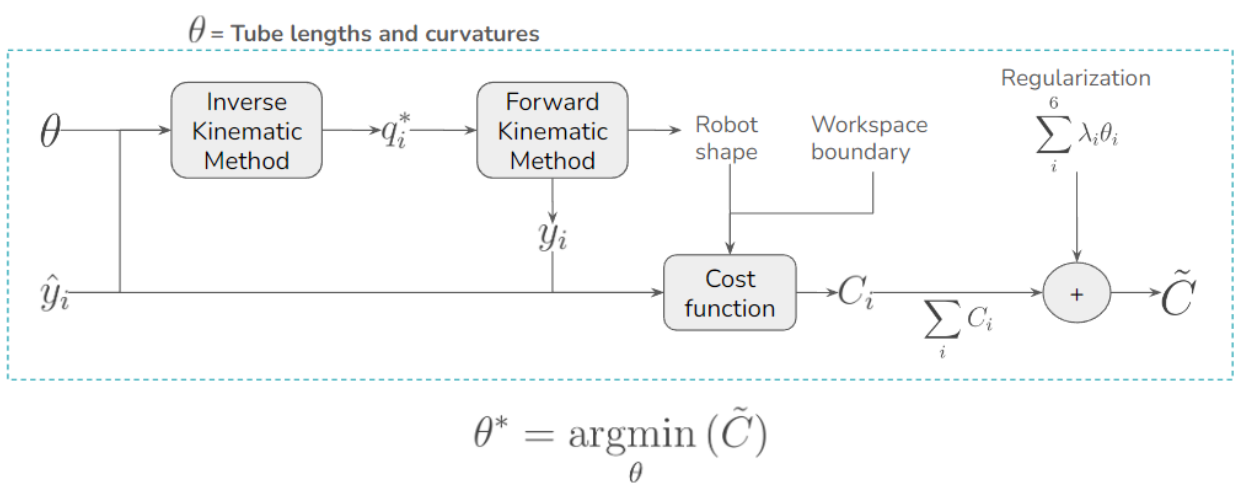

Figure 21: Tube parameter optimization process

Given a series of test points $\{\hat{y}_i\}_1^N$ and a set of physical tube parameters (extension lengths, curved lengths, curvatures) expressed as a vector θ, we can use the algorithm outlined in Fig. 21 to

determine the tube parameters that will optimize the robot's range of motion within the workspace boundary (an S-shaped pipe in our case). For a given set of tube parameters, we see how close the robot can get to each test location and penalize it for not obeying the workspace boundaries (i.e. hitting the walls of the pipe). The error from the deviation of the tip position and orientation from the test point and the penalty for boundary infringements are wrapped into a cost function which is summed across all test points and added to a regularization term to limit any extreme lengths or curvatures. This metric is then minimized to determine the optimal tube parameters. While this process could be further optimized, the results we obtained explored our theoretical workspace sufficiently well for our purposes. The implementation of Fig. 21 is detailed in our GitHub.

D Bill of Materials

Item Description and Supplier Link	**CAD excl.tax, excl.ship.**
Rail Guide (1m) and Pillow Blocks (x12)	$248.57
Closed Loop Stepper Motors (x6)	$156.00
Closed Loop Stepper Drivers (x6)	$267.63
Output Gear (x6)	$86.40
Driver Gear (x6)	$128.58
Translation Bearings (x6)	$80.64
Rotation Bearings A (x3)	$19.53
Rotation Bearings B (x3)	$52.53
Bidirectional Logic Level Converter (x5)	$17.50
Endoscopic Camera	$103.23
M3 x 12mm BHCS bolts pack of 100	$7.06
Total	**$1,167.67**

Table 3: Bill of Materials

References

Alqumsan, A. A., Khoo, S., and Norton, M. (2019). Robust control of continuum robots using cosserat rod theory. *Mechanism and Machine Theory*, 131:48–61.

Baron, A. (2022). How to shape set nitinol. `https://www.kelloggsresearchlabs.com/2020/06/24/shape-setting-nitinol/`.

Bergeles, C., Gosline, A. H., Vasilyev, N. V., Codd, P. J., del Nido, P. J., and Dupont, P. E. (2015). Concentric tube robot design and optimization based on task and anatomical constraints. *IEEE Transactions on Robotics*, 31(1):67–84.

Burgner-Kahrs, J., Rucker, D. C., and Choset, H. (2015). Continuum robots for medical applications: A survey. *IEEE Transactions on Robotics*, 31(6):1261–1280.

Dupont, P. E., Lock, J., Itkowitz, B., and Butler, E. (2010). Design and control of concentric-tube robots. *IEEE Transactions on Robotics*, 26(2):209–225.

Dupont, P. E., Simaan, N., Choset, H., and Rucker, C. (2022). Continuum robots for medical interventions. *Proceedings of the IEEE*, 110(7):847–870.

Euroflex (2021). *Technical Specifications*. Euroflex. `https://www.euroflex.de/fileadmin/content/Dokumente/Datenblaetter/technical_spec_1-quer_sep_seite_E.pdf`.

feng ZENG, Q., meng ZHAO, X., neng DONG, G., and xing WU, H. (2012). Lubrication properties of nitinol 60 alloy used as high-speed rolling bearing and numerical simulation of flow pattern of oil-air lubrication. *Transactions of Nonferrous Metals Society of China*, 22(10):2431–2438.

Gilbert, H. B. and Webster, R. J. (2016). Rapid, reliable shape setting of superelastic nitinol for prototyping robots. *IEEE Robotics and Automation Letters*, 1(1):98–105.

Grassmann, Chengnan, Hamoda, Triana, and Burgner-Kahrs (2024). Open continuum robotics–one actuation module to create them all. *Frontiers in Robotics and AI*, 11.

Grassmann, R. M., Chen, R. Z., Liang, N., and Burgner-Kahrs, J. (2022a). A dataset and benchmark for learning the kinematics of concentric tube continuum robots.

Grassmann, R. M., Chen, R. Z., Liang, N., and Burgner-Kahrs, J. (2022b). A dataset and benchmark for learning the kinematics of concentric tube continuum robots.

Liu, T., Zhang, G., Zhang, P., Cheng, T., Luo, Z., Wang, S., and Du, F. (2023). Modeling of and experimenting with concentric tube robots: Considering clearance, friction and torsion. *Sensors*, 23(7).

Matthey, J. (2024). Nitinol shape setting. `https://matthey.com/products-and-markets/other-markets/medical-components/resource-library/nitinol-shape-setting#:`

~:text=In%20general%2C%20temperatures%20as%20low,and%20the%20fixture%20are%20small).

Motion, D. (2023a). Motion control handbook: Microstepping. https://dovermotion.com/resources/motion-control-handbook/microstepping/#:~:text=The%20torque%20which%20any%20microstep,is%20the%20step%20division%20ratio.

Motion, D. (2023b). Motion control handbook: Resolution. https://dovermotion.com/resources/motion-control-handbook/resolution/.

Nwafor, C. J., Girerd, C., Laurent, G. J., Morimoto, T. K., and Rabenorosoa, K. (2023). Design and fabrication of concentric tube robots: A survey. *IEEE Transactions on Robotics*, 39(4):2510–2528.

Russo, M., Sadati, S. M. H., Dong, X., Mohammad, A., Walker, I. D., Bergeles, C., Xu, K., and Axinte, D. A. (2023). Continuum robots: An overview. *Advanced Intelligent Systems*, 5(5):2200367.

Sears, P. and Dupont, P. (2006). A steerable needle technology using curved concentric tubes.

StepperOnline (2023). *CL57T Closed-loop Stepper Driver Manual*. https://www.omc-stepperonline.com/index.php?route=product/product/get_file&file=3152/CL57T-V41%20Manual.pdf.

Webster III, R. J. and Jones, B. A. (2010). Design and kinematic modeling of constant curvature continuum robots: A review. *The International Journal of Robotics Research*, 29(13):1661–1683.

Wikipedia (2023). Euler–bernoulli beam theory. https://en.wikipedia.org/wiki/Euler%E2%80%93Bernoulli_beam_theory.

Yedamale, P. (2003). An885, brushless dc (bldc) motor fundamentals. https://ww1.microchip.com/downloads/en/AppNotes/00885a.pdf.

Yip, M. C., Alaie, S., Romito, E. A., Doshi, T., Amiri Moghadam, A. A., Mosadegh, B., and Dunham, S. (2023). Low-cost and rapid shaping of nitinol for medical device prototyping. *ASME Open Journal of Engineering*, 2.

Zeng, Q. and Dong, G. (2013). Influence of load and sliding speed on super-low friction of nitinol 60 alloy under castor oil lubrication. *Tribology Letters*, 52(1):47–55.